Applicability of Strain Softening Analysis for Tunnel Excavation

Kenichi NAKAOKA* and Hiroaki KITOH**

(Received October 2, 2015)

Synopsis

As a one of alternative model to predict the behavior of tunnel excavation in unconsolidated ground, the strain hardening up to softening model has been proposed in this paper. The model based on plastic theory has been formulated, not in ordinary stress space but in strain one because of consistent unloading definition due to strain softening. Material model parameters were estimated from unconfined and tri-axial compression tests. After the defined model parameters applied into FEM procedure, centrifuge test model has been simulated. As the results, obtained surface settlement and lateral face displacement were well agreed with experimental results. Furthermore, the distribution of predominant shear strain around tunnel obtained was also comparable with the sliding phenomena observed in the experimental test. In conclusion, the proposed model can be applicable to tunnel stability problem in unconsolidated ground.

KEYWORDS: Strain softening, Lade model, Finite element analysis, Tunnel face stability, Strain-space

1. Introduction

New Austrian Tunneling Method: NATM is being increasingly used for excavation of shallow tunnels within unconsolidated soils. The main reason is that the lower cost for tunnel construction than that by shield tunneling method and lower impact for traffic than that by open cut method around the construction site.

Some reports have indicated that a tunnel excavation by NATM within unconsolidated soil often expands the high shear zone, called, “shear band,” from the tunnel sides upward[1)]. And by experiment it was shown that the “shear band” expands also from tunnel face towards surface samely[2)]. If this zone approaches the surface, it can cause large settlement of surface above the tunnel and lead to tunnel collapse in the worth case. Therefor a numerical model is required that can simulate the expanding of the shear band to determine the stability of a tunnel in unconsolidated soil. Usually, however, normal elastic[ex.3)] or elasto-plastic models[ex.4)] are used in the analysis of tunnel stability, so it is insufficient to evaluate behavior of ground around the tunnel. It is not easy to observe the extension of actual shear bands or to simulate experimentally. So, validation of strain softening model for the evaluation of extension of shear band is not progressing. It is considered the reason that the model does not become widely used as the analysis method for a design. Therefore, it is important to increase the validation example about the extension of shear band.

Lee[5)] and Akutagawa[6)] developed a strain softening model to predict ground behavior taking into account the shear band caused by tunnel excavation. And applied to evaluation the expanding of shear band from actual tunnel sides upward. After that, it was shown that the strain softening model can simulate the surface settlement that was considered to have been caused by the shear band. Nakaoka et al[7)] expanded the model to three dimensional problem, and it was shown that the model can simulate the discontinuous displacement developed from tunnel face in centrifugal experiment that was carried out by Takahashi et al[8)].

The manner of this model is that, if material yielded, stress is redefined by shrinking of Mohr’s stress circle to fit into the Mohr-Coulomb criterion line. The strain softening is taken account by reducing the cohesion and internal frictional angle according to maximum shear strain. Also, the anisotropy is considered by decreasing of shear stiffness on local coordinates along a slip line in consideration of shear band developing. The model doesn’t use dilatancy parameter, so the model became simple mathematically, and increase a practicality.

On the other hand, it is considered that the numerical model based on plastic theory that was developed for simulation of the soil behavior will become one of the choices for design of tunnel in unconsolidated ground. However the numerical model like that was not investigated whether it can simulate correctly the shear band around the tunnel. Then, we focused on the numerical model that was developed by Lade[9)] (Lade model). This model intended for evaluation of non-cohesive sandy soil. And by taking into the plastic work as an index, this model can simulates strain hardening and softening seamlessly.

The model is newly added the cohesion term for cohesive soil. A strain-space-based plasticity formulation

* Student, Doctor Course of Department of Civil Engineering (Obayashi Corporation)

** Professor, Department of Urban Engineering, Osaka City University

is used to represent strain hardening and softening behavior completely. After that the numerical model is mounted on the code of finite element method (FEM), and applicability is ascertained by simulating about the centrifuge tests of tunnel model.

In this paper, at first, Lade model that takes into account of cohesion is outlined. And, the parameters such as for strain hardening and softening are estimated by fitting to strain-stress curve of unconfined and tri-axial compression tests using the same compounding material with soil in tunnel model. After that, the centrifuge model tests[8] are simulated with parameters obtained as previously shown, and by comparing analysis results with model tests, applicability of the numerical model is discussed.

2. Strain hardening and softening model

(1) Strain softening model

Lade proposed an elasto-plastic constitutive model that was specified the strain hardening and softening formation to present the nonlinear behavior of non-cohesive soil[6]. Using parameters of the numerical model that was estimated by tri-axial compression tests, he showed that the model can simulate well the strain hardening and softening behavior of non-cohesive soil. Mizuno[10] studied about applying the model on concrete material, the strain hardening and softening behavior of concrete in tri-axial compression test under low confined stress which was from 0.3 to 1.2% of uniaxial compressive strength was simulated[7]. Mizuno described an elasto-plastic constitutive law that involves strain hardening and softening should be formulated in strain-space.

In this study, we apply the Lade model modified by Mizuno using strain-space-based plasticity formulation. Denoting that the loading function f in stress-space and F in strain-space respectively, and corresponding increment df and dF according to increment of stress $d\sigma_{ij}$ and increment of strain $d\varepsilon_{ij}$ are represented as shown in Eq.1 and Eq.2.

$$df = \frac{\partial f}{\partial \sigma_{ij}} d\sigma_{ij} \tag{1}$$

$$dF = \frac{\partial F}{\partial \varepsilon_{ij}} d\varepsilon_{ij} \tag{2}$$

As shown in right half of Fig.1, when $df > 0$, it means hardening by loading. On the other hand, when $df < 0$, it means elastic unloading or unloading by softening. It cannot determine which is the real state of unloading only by the stress. As shown in left half of Fig.1, applying the loading function defined in strain space, it means elastic unloading with $dF < 0$. On the other hand, it means hardening or softening by loading with $dF > 0$. There is no need to distinguish which is the state of loading. Strain hardening and softening are described in constitutive law continuously in strain space. Thus, the problem seen in formulation in stress space can be solved. Loading function applied in this study is represented by Eq.3 in stress-space.

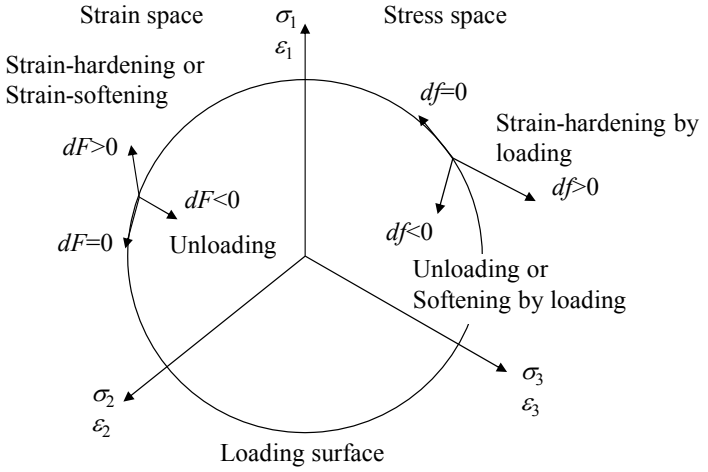

Fig.1 Stress state in stress-space and strain-space

$$f = (I_1 + a)^3 - \left(27 + f_p\left(\frac{P_a}{(I_1 + a)}\right)^m\right) \times \left(\frac{1}{27}(I_1 + a)^3 - \frac{1}{3}(I_1 + a)J_2 + J_3\right) = 0 \tag{3}$$

Here, the meanings of the parameters in equation are shown below:

a: As shown in Fig.2, the amount of parallel shift of the yield surface along hydrostatic axis in tensile direction.

m: Curvature of the yield surface. If $m = 0$, the distance between yield surface and hydrostatic axis becomes linear relationship with respect to hydrostatic pressure. If $m > 0$, the relationship becomes concave down with respect to hydrostatic pressure. And if $m < 0$, the relationship becomes concave up.

f_p: Strain hardening and softening, parameter, which is defined as a function of plastic work W_p. The parameter defines the material strength, the value is 0 initially. It increases owing to hardening and becomes maximum value η_1 when the corresponding stress attains at its peak. Afterward, it decreases with softening.

P_a: pressure of the atmosphere.

I_1, J_2, J_3 are the stress invariants, these are shown in Eqs.4 ~ 6, respectively, using strain invariants.

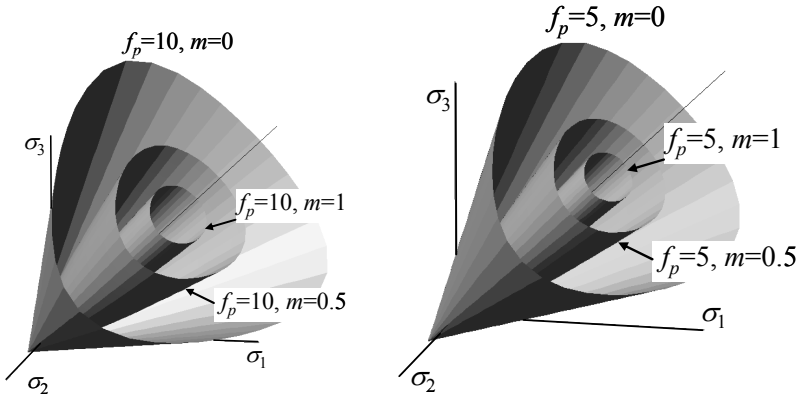

Fig.2 Lade loading surface according to m and f_p

$$I_1 = \sigma_{ii} = 3K(\varepsilon_{ii} - \varepsilon_{ii}^p) = 3K\overline{I_1} = \overline{A}\overline{I_1} \tag{4}$$

$$J_2 = \frac{1}{2}s_{ij}s_{ij} = 2\mu^2(e_{ij} - e_{ij}^p)(e_{ij} - e_{ij}^p) = \overline{B}\overline{J_2} \tag{5}$$

$$J_3 = \frac{1}{2}s_{ij}s_{jk}s_{ki} = \frac{8}{3}\mu^3(e_{ij} - e_{ij}^p)(e_{jk} - e_{jk}^p)(e_{ki} - e_{ki}^p) = \overline{C}\overline{J_3} \tag{6}$$

The loading function in strain space is described as Eq.7.

$$\mathrm{F} = \left(\overline{\mathrm{A}}\overline{I_1} + a\right)^3 - \left(27 + \mathrm{f_p}\left(\frac{P_a}{\left(\overline{\mathrm{A}}\overline{I_1} + a\right)}\right)^m\right) \times \left(\frac{1}{27}\left(\overline{\mathrm{A}}\overline{I_1} + a\right)^3 - \frac{1}{3}\left(\overline{\mathrm{A}}\overline{I_1} + a\right)\overline{\mathrm{B}}\overline{J}_2 + \overline{\mathrm{C}}\overline{J}_3\right) = 0 \tag{7}$$

$$\overline{A} = 3K \tag{8}$$

$$\overline{B} = 4\mu^2 \tag{9}$$

$$\overline{C} = 8\mu^3 \tag{10}$$

Where, ε_{ij}^p, e_{ij}, e_{ij}^p means plastic strain, deviator strain, deviator plastic strain respectively. K and μ are elastic volumetric modulus and shear modulus, respectively

$$K = \frac{1}{3(1-2\nu)} \tag{11}$$

$$\mu = \frac{1}{2(1+\nu)} \tag{12}$$

(2) Procedure of non-linear calculation

A finite element method: FEM is used for this study. The method of calculation of non-linearity is to apply a gradually increasing load. Fig. 3 is the flowchart of the calculation.

Modified Newton Raphson scheme is employed to converge residual force. The scheme is as follows: At first, overall stiffness matrix K is made, and strain increment $\Delta\varepsilon$ is obtained with K and increment of load Δf_{load}. Next, plastic strain $\Delta\varepsilon^{\text{p}}$ is obtained by elasto-plastic constitutive equation using the previous values of $\Delta\varepsilon$, and ε^{e} and W_{p} to be explained in detail. Now, it is possible to obtain the current stress increment: $\Delta\sigma=D\Delta\varepsilon^{\text{e}}$, where D is elastic stiffness matrix, and $\Delta\varepsilon^{\text{e}}=\Delta\varepsilon - \Delta\varepsilon^{\text{p}}$ is relevant elastic strain in increment. Then the current stress: σ updated owing to the obtained increment. Residual force of next step is estimated from σ obtained as above. Stress of next step is obtained by loading the residual force. Again, σ is changed by the $\Delta\sigma$ that is calculated under new σ. Residual force generated by stress change is calculated again. When the maximum residual force becomes less than allowable value, the calculation is terminated.

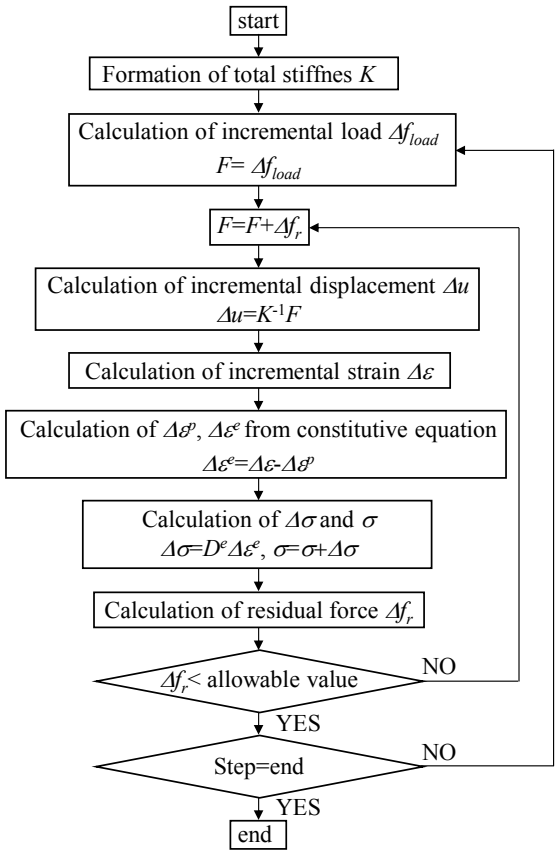

Fig.3 Flowchart of non-linear analysis

3. Defining of model parameters

(1) The parameters and procedure of definition

The parameters were defined using the results of unconfined and tri-axial compression test. Test specimens had the same composition as the material applied to the centrifuge model experiment[8]. The material was soil cement as mixture of low plasticity kaolin clay and cement. Kaolin clay is an article on the market, which plastic index: IP=10%. Cement content was 100kg/m^3 to become the unconfined compressive strength 70kPa of target strength. Fig. 4 shows the proceeding of each parameters definition.

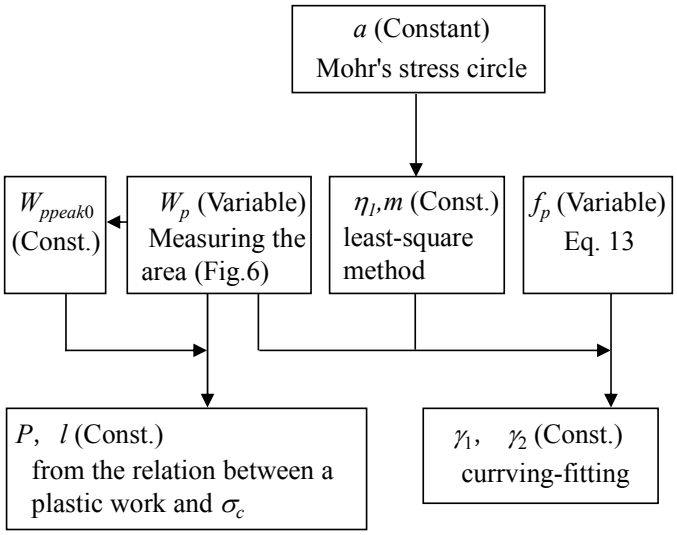

Fig.4 Procedure of parameters setting

Material parameters were as follows: Young's modulus E=16.6MPa, Poisson's ratio ν=0.4, and as the parameters that define the loading function, a and m these define the shape of curved surface, f_p that is the parameter of material strength, η_1 that defines the maximum value of f_p, and the parameters W_{ppeak0}, P, l, γ_1, γ_2 to link f_p and plastic work W_p. Eq. 13 shows the relation between f_p and W_p. The number of the essential parameters was eight.

$$f_p = \eta_1 \left(\frac{e \cdot P_a}{W_{ppeak}}\right)^{\frac{1}{\gamma}} \times \exp\left(-\frac{W_p}{\gamma W_{ppeak}}\right) \times \left(\frac{W_p}{P_a}\right)^{\frac{1}{\gamma}} \tag{13}$$

$$W_{ppeak} = P\left(\frac{\sigma_c}{P_a}\right)^l P_a + W_{ppeak0} \tag{14}$$

$$\gamma = \gamma_1 \sigma_c + \gamma_2 \tag{15}$$

Here, σ_c is confined pressure of the triaxial compressive test. On the FEM calculation, the average of maximum principal stress and intermediate principal stress was used as confined pressure in which negative value means compression. The relation between strain and stress that was obtained by the unconfined compression test and the triaxial compression test is shown together with the results of calculation later. And to be consistent with the results of the uniaxial compression test, it was multiplied by a constant on the results of the triaxial compression test. To define the parameter, the results obtained in this way were used.

(2) Definition of each parameter a, m, η_1

The first parameter a is the shift distance of curved surface of loading function along the hydrostatic axis as Fig.2, which was estimated as the intersection point of envelope line and σ axis shown in Fig.5. The parameter a is an absolute value. From Fig.5, it was estimated to be 532kPa.

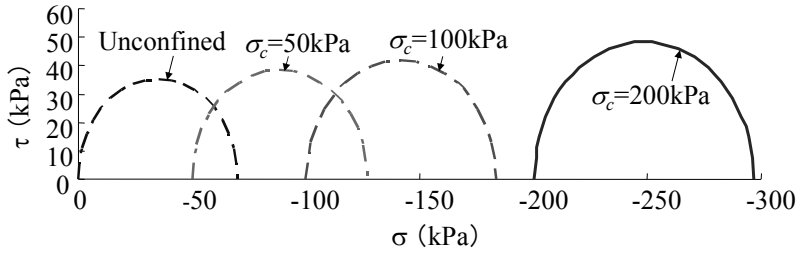

Fig.5 Mohr's stress circle at each confining stress

The parameter η_1 and m represent peak strength and curvature of loading surface respectively; those were estimated by the assigning parameter a that described above to plastic-potential function. After that, parameter m and η_1 were adjusted to minimize the standard variation of η_1 that is obtained by each of the element tests. From element tests, it was set to m=1.08, η_1=7.10.

(3) Definition of each parameters W_{ppeak0}, P, l

Plastic work is estimated from strain-stress curve obtained from the compression tests. Here, it is assumed that the material is in elastic state when unloading. The plastic work can be obtained by measuring the area of hatching in Fig.6.

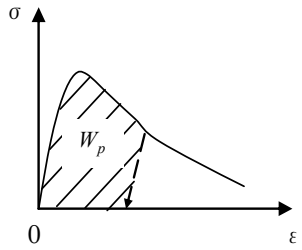

Fig.6 Work of plasticity

W_{ppeak} is the plastic work when difference of principal stress by tri-axial compression test becomes maximum. W_{ppeak0} is also the plastic work when axial stress of unconfined test becomes maximum. Table 1 shows the W_{ppeak0} values estimated from the results of each test. By using the parameters of W_{ppeak0}, P and l, W_{ppeak} under confined pressure σ_c can be calculated by Eq.14. From relationship between $(W_{ppeak0} - W_{ppeak})/P_a$ and σ_c/P_a in double logarithmic plot shown in Fig.7, P and l were estimated by least-square technique as P=0.00779 and l=0.761. If the values of W_{ppeak0}, P and l are increased, strain at peak stress is increased.

Table 1 W_{ppeak} (kPa)

Confined Pressure σ_c (kN/m^2)	W_{ppeak}
0	0.66
50	1.07
100	1.56
200	1,82

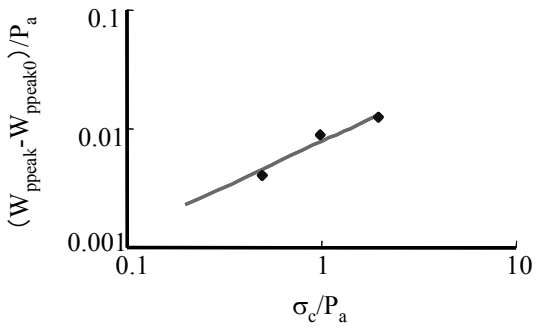

Fig.7 Relation of $(W_{ppeak0} - W_{ppeak})/P_a$ and σ_c/P_a

(4) Definition of each parameters γ_1, γ_2

Among the parameters included in the function f_p shown by Eq.3, γ value mainly defines the gradient of strain-stress curve after peak. It is assumed that γ is proportional to the confining pressure σ_c as shown by Eq.15. Procedure of defining γ is as follows. At first, measured value f_p is calculated by assigning the parameters a and m to the loading function that is shown as Eq.3. Next, the parameters η_1, W_{ppeak0}, P and l are assigned into Eq.13 and Eq.14. And by curve-fitting which is done to conform the calculated value of f_p to the measured value, γ is estimated. Fig. 8 shows the results of the curve-fitting. γ obtained under each confining pressures are shown in Fig.9. However, γ becomes large value unrealistically because softening did not occurred almost in the case of the confining pressure=200kPa. So the case was eliminated. Parameter γ_1 as the gradient of relationship between σ_c and γ was defined as 0.130 from the figure. Also, the intercept γ_2 was defined as 0.453. Table 2 shows the parameters set as explained.

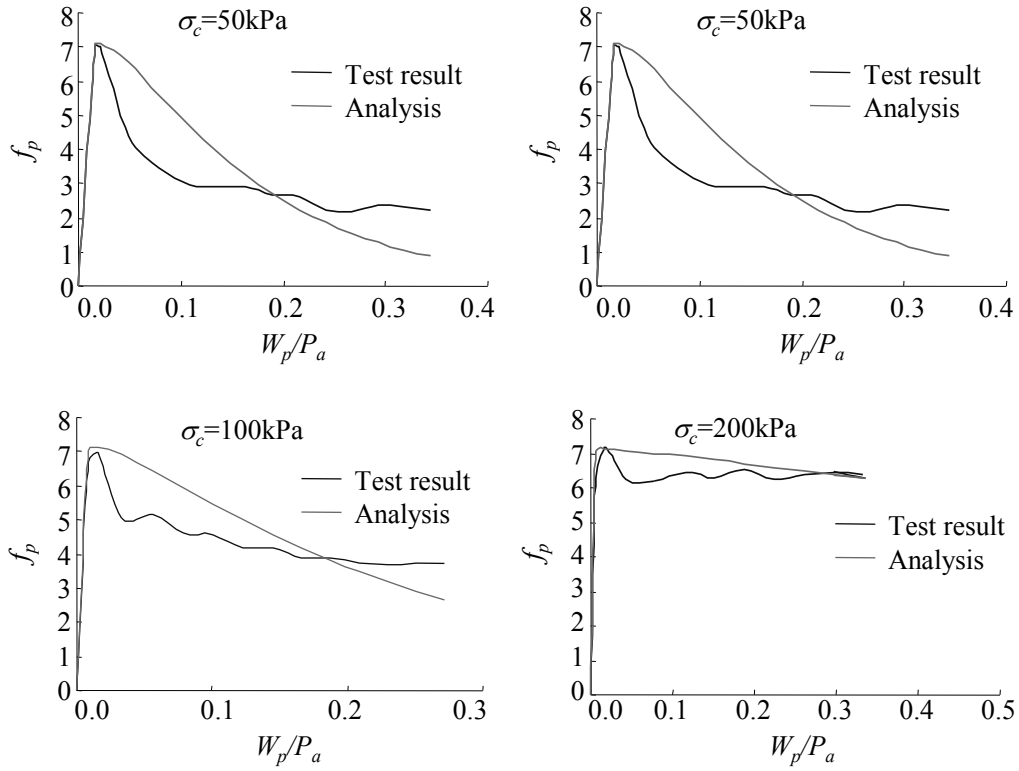

Fig.8 Relationship between W_p and f_p that obtained by curve-fitting

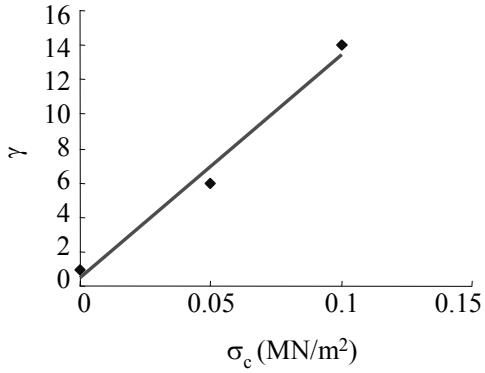

Fig.9 Relationship between γ and σ_c

Table 2 The parameters for numerical simulation

Parameters	value
the amount of parallel shift (a)	0.532 MPa
Degrees of loading function curvature (m).	1.08
the maximum value of f_p (η_1)	7.1
Relation between W_{ppeak} and σ_c (P)	0.00779
Relation between W_{ppeak} and σ_c (P)	0.761
Relation between f_p and W_p (γ_1)	130 m^2/MN
Relation between f_p and W_p (γ_2)	0.453
The value of W_{ppeak} at σ_c =0	6.57×10^{-4}MPa
Atmospheric pressure (P_a)	0.101 MPa
Young's modulus (E)	16.6MPa
Poisson's ratio (ν)	0.4
Density (ρ)	1740 kg/m^3

4. The results of numerical analysis

(1) The results of simulation of element test

Fig. 10 shows the results of both simulation of the unconfined compression tests and the tri-axial compression tests. The results of simulations of unconfined tests were similar with the test results. The results of peak strength by simulation of tri-axial compression tests were also similar with the test results. The obtained gradients after peak, however, were slower than those from the test results.

As shown in Fig. 8, we tried to fit the simulation results with actual measurement, but a difference still remained. It is considered that this is the reason of difference between numerical simulation and test results in Fig. 10. Because peak stress is in agreement, and analysis results approach test results as strain increases, we expected that the numerical analysis could obtain the similar results with the experiment.

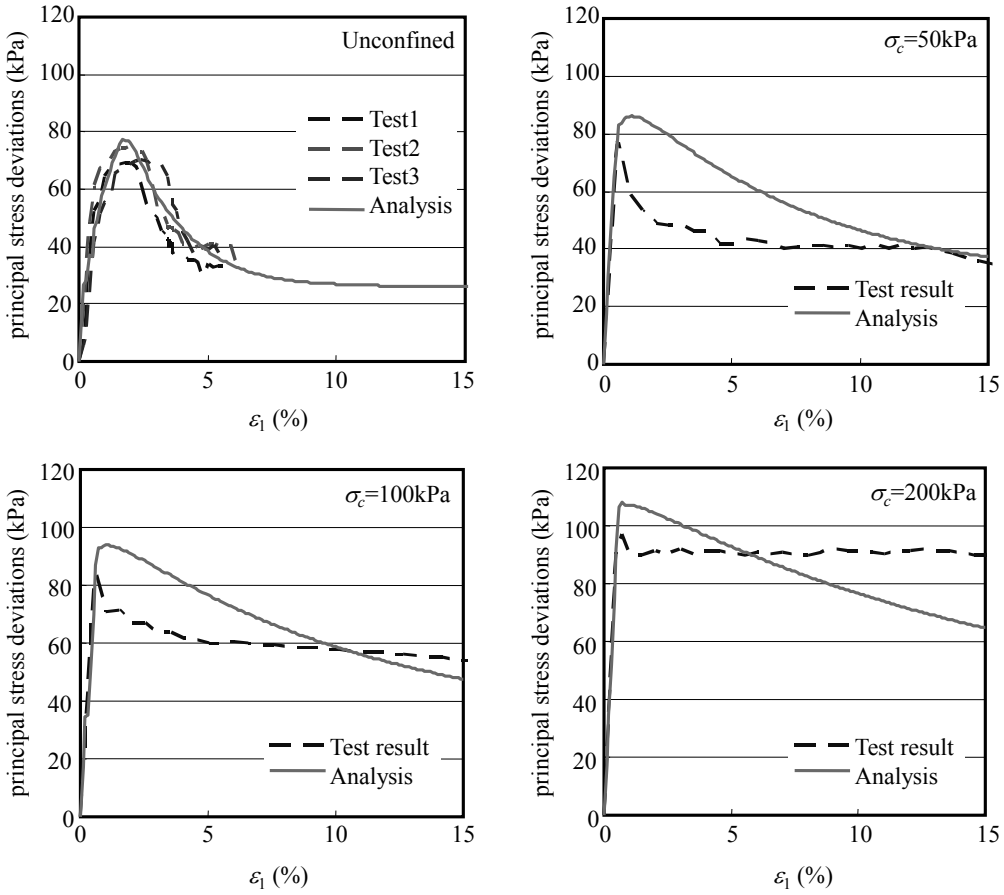

Fig.10 The results of simulation of unconfined compression and triaxial compression tests

(2) Numerical simulation of centrifuge model tests

(a) Outline of the tests

The tunnel model for centrifuge is shown in Fig.11 and Fig.12[8]. Model ground was installed in steel container, called container hereafter as shown in Fig.12. The half hole was created in the model ground as the tunnel face from the start. After that, centrifugal acceleration was gradually increased up to 80G. The shape of tunnel is hemicycle and its diameter was 10cm as shown in Fig.11. When acceleration attained to 80G, It correspond to tunnel diameter of 8m and earth covering of 16m. The tunnel was regarded as a half pipe of right side toward the tunnel face. Tunnel body except 5cm interval close to the face was supported by acrylic half pipe. The support prevented a collapse of tunnel body before the collapse of tunnel face focusing on in this experiment. Front face of container was covered by acrylic board to measure the displacement of ground through the board.

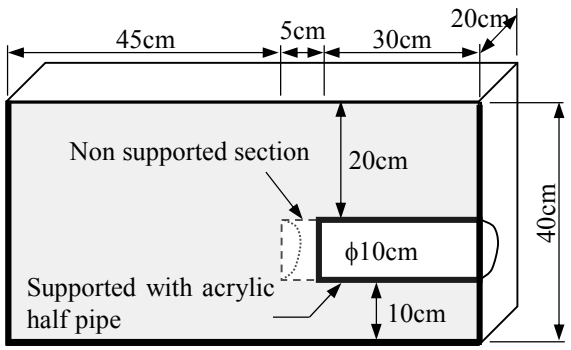

Fig.11 Tunnel face of centrifuge model tests

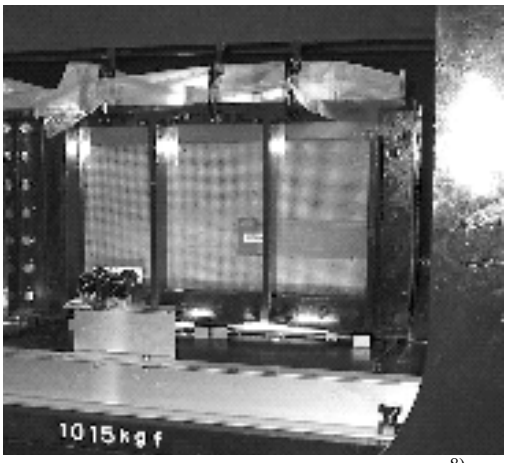

Fig.12 The model on loading stage[8)]

Settlement of ground surface just above the tunnel face and lateral displacement of center of tunnel face were measured. It is targeted the experiment condition close to undrained by not installing the drainage in the container.

(b) Analytical model

Fig. 13 shows analytical model, in which the view point of displacement for comparison with the experiment is shown. Dimension of analysis model was same as the experimental model.

Tunnel supporting was also modeled by solid elements as shown in Fig.13, and the relevant elements were assigned enough high elasticity compared to elements for ground. As the boundary condition, displacement of model bottom was fixed, and normal direction of surface around the model was also fixed. It is not assigned boundary condition in ground surface. All load of numerical analysis was dead load of ground. Gravity acceleration was increased gradually up to 80G as same as the experiment. The total number of increment step was 100.

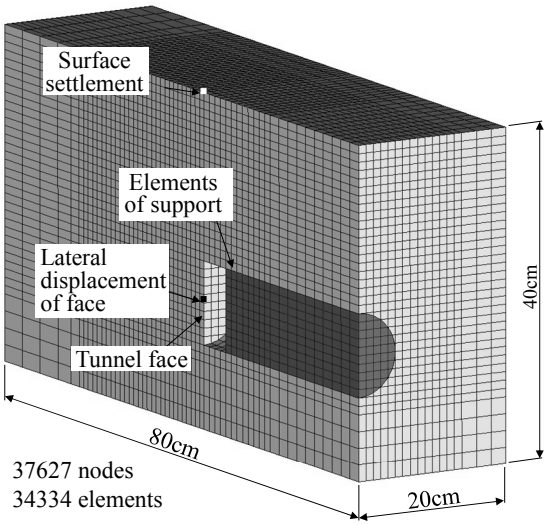

Fig.13 Finite element mesh

(c) Analysis results

Fig. 14 shows relation between centrifuge acceleration and settlement, and also another relation between acceleration and lateral displacement. For reference, it also shows the results of elastic analysis. From the experimental results (○), we can see the rapidly increasing of displacement at about 55G. Elastic analysis indicated with straight lines could not follow naturally such the behavior. On the other hand, settlement gradient of analysis indicated with blue line curve increased at about 50G. Finally, the obtained settlement reached 16mm at 80G. It can be seen that the analysis evaluated the settlement obtained by experiment well.

Lateral face displacement of the experiment rapidly increased at about 55G similarly with the settlement. After that, at about 70G, a crack extended from bottom of the face upward. Finally it caused a collapse.

According to analysis indicated with red curve, lateral displacement increased rapidly at about 50G. It simulated well the lateral face displacement of the experiment.

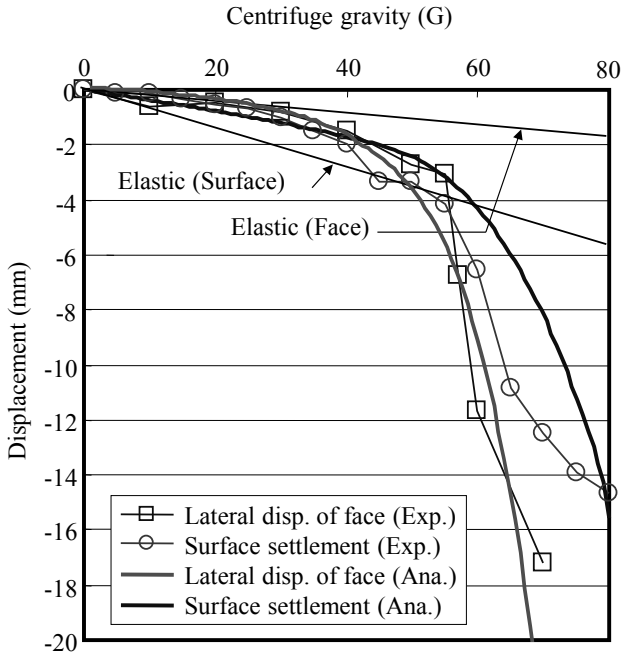

Fig.14 Comparison between results of analysis and experiment

Fig. 15 shows the crack location obtained by experiment when acceleration was 50G. Also, the distribution of maximum shear strain at 50G obtained by analysis is shown together.

At 40G, crack as broken line in experimental model extended upward from bottom of the tunnel face where the stress concentrated. At 50G, the crack as solid line reached to crown of the face. As the obtained result, shear strain in the bottom and top of the tunnel face was larger than 5%. Crack and large shear strain area were limited in location close to the face in this stage. We could not find the behavior that these region extending upward beyond the face crown.

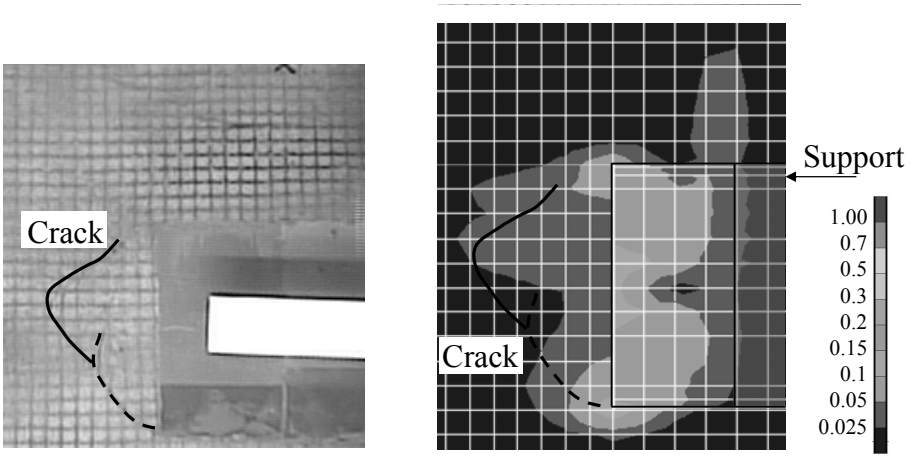

Fig.15 Left: cracking of the experimental model in 50G[8)], Right: distribution of maximum shear strain by analysis in 50G

Fig. 16 shows the experimentally obtained crack location and calculated maximum shear strain distribution at 80G. With the experimental model, crack extended upward from bottom of tunnel face, and finally it led the collapse of tunnel face. Also, crack extended vertically from the edge of near the tunnel face. Also by the analysis, high strain region extended upward from front of the tunnel face and from edge of acrylic support, the region which is called shear band. So, it could be drawn that the numerical model simulates the behavior of the experimental model well.

The crack from the edge of acrylic support in the experimental model did not reach to surface of ground. On the other hand, the shear band in analysis reached to surface. The reason of this difference is that there are some blocks fell into the tunnel discontinuously from around of the tunnel face in the experimental model. So, mass load of fell blocks do not apply to upper ground of tunnel.

On the other hand, a behavior that fall of discontinuous block cannot be simulated in the numerical model, so the load acting on the upper ground does not decrease. It is considered that the load acting on upper ground of numerical model become larger than experiment. So shear band in the numerical model reached to surface whereas crack in the experimental model did not reach.

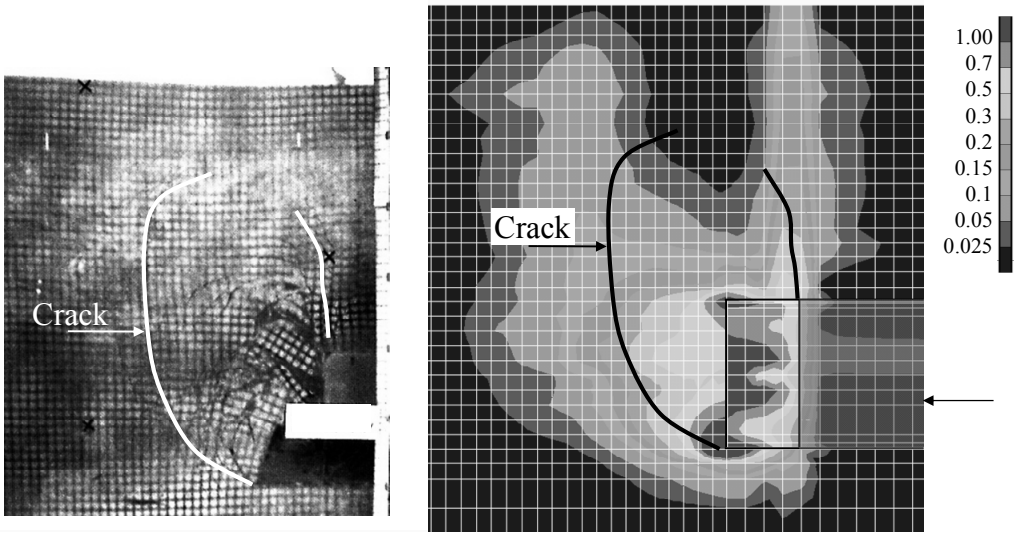

Fig.16 Left: cracking of the experimental model in 80G[8)], Right: distribution of maximum shear strain by analysis in 80G

Fig. 17 shows the displacement by analysis at 80G. From the figure, it can be seen that ground of front of tunnel face displaces like flow in the direction of the tunnel.

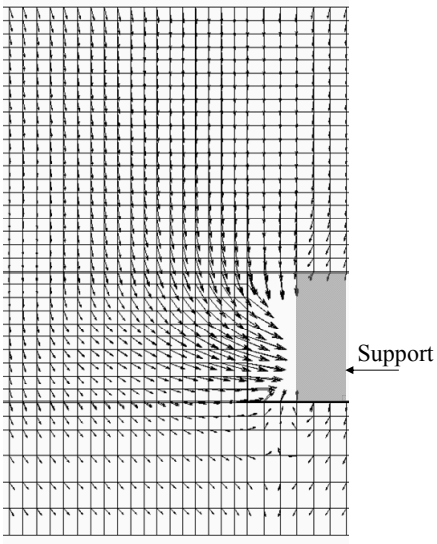

Fig.17 Displacement vector by analysis at 80G

5. Conclusion

In this study, to evaluate the applicability of strain softening-hardening model to problem of stability of tunnel face in unconsolidated ground with shear band extensions, Lade type elasto-plastic model that is added cohesion term is applied.

At first, unconfined compression tests and tri-axial compression tests with same composition specimen of centrifuge ground model are simulated by numerical model. And by fitting results to elemental tests, eight parameters are estimated. After that, centrifuge model tests are simulated. The results of these, the relation between lateral face displacement and centrifuge acceleration and relation between surface settlement and acceleration are estimated well. Also, location of crack developed in experimental model is well predicted as shear band by numerical model.

By using the method of evaluate the nonlinearity by modifying the stress, Lade type elasto-plastic model that predict the strain softening and hardening can be applied to problem of tunnel stability. It can be determined that it becomes an option in the case of tri-axial compression test data is available.

6. References

1) W. H. Hansmire, and E. J. Cording, *J. Geotech. Eng.*, **111**, 1301 (1985)
2) D. Steripi, and A. Cividini, *Rock Mech. Rock Eng.*, **37**, 277 (2004)
3) H. Ohtsu, Y. Hakoishi, M. Nago, and H. Taki, *Proceedings of the South East Asian Symposium on Tunneling and Underground Space Development*, 157-164 (1995)
4) S. Abdel-Baki, A. Ata and M. Hamza, *Proceedings of the North American Tunneling '96*, 11 (1996)
5) J. Lee, S. Akutagawa, T. Kitagawa, A. Isogai, and T. Matsunaga, *Proceeding of Tunnel Engineering*, **15**, 69 (2005)
6) S. Akutagawa, K. Matsumoto, and H. Nagai, *Proceeding of Tunnel Engineering*, **10**, 113 (2000) (in Japanese)
7) K. Nakaoka, K. Hata, S. Akutagawa, and S. Takahashi, *Proceeding of 2nd International Conference on Computational Methods in Tunneling*, **2**, 281 (2009)
8) S. Takahashi, S. Sugie, T. Kuwahara, and M. Toriihara, *Proceeding of the Japan National Conference on Geotechnical Engineering*, **40**, 1867 (2005) (in Japanese)
9) P. V. Lade, *Int. J. Solid Struct.*, **13**, 1019 (1977)
10) E. Mizuno, and S. Hatanaka, J. Eng. Mech.-ASCE, **118**, 1546 (1992)